ATMOSPHERIC SCIENCE LETTERS
Atmos. Sci. Let. (2017)
Published online in Wiley Online Library
(wileyonlinelibrary.com) **DOI:** 10.1002/asl.729

RMetS
Royal Meteorological Society

Intraseasonal rainfall variability in the Bay of Bengal during the Summer Monsoon: coupling with the ocean and modulation by the Indian Ocean Dipole

Siraput Jongaramrungruang,[1,2,3] Hyodae Seo[2*] and Caroline C. Ummenhofer[2]

[1] *Trinity College, University of Cambridge, UK*
[2] *Physical Oceanography Department, Woods Hole Oceanographic Institution, MA, USA*
[3] *Now at Division of Geological and Planetary Sciences, California Institute of Technology, CA, USA*

**Correspondence to:*
H. Seo, 266 Woods Hole Road, MS#21, Woods Hole, MA 02543, USA.
E-mail: hseo@whoi.edu

Received: 26 August 2016
Revised: 9 December 2016
Accepted: 15 December 2016

Abstract

The Indian Summer Monsoon rainfall exhibits pronounced intraseasonal variability in the Bay of Bengal (BoB). This study examines the intraseasonal rainfall variability with foci on the coupling with sea surface temperatures (SST) and its interannual modulation. The lagged composite analysis reveals that, in the northern BoB, SST warming leads the onset of intraseasonal rainfall by 5 days. Latent heat flux is reduced before the rain event but is greatly amplified during the rainfall maxima. Further analysis reveals that this intraseasonal rainfall-SST relationship through latent heating is strengthened in negative Indian Ocean Dipole (IOD) years when the bay-wide local SST is anomalously warm. Latent heat flux is further increased during the intraseasonal rainfall maxima leading to strengthened rainfall variability. The moisture budget analysis shows this is primarily due to stronger low-level moisture convergence in negative IOD years. The results provide important predictive information on the monsoon rainfall and its active/break cycles.

Keywords: **Bay of Bengal; intraseasonal; monsoon; IOD**

1. Introduction

During boreal summer (June to September, JJAS), strong southwesterly monsoon winds carry moisture from the tropical Indian Ocean onto the Indian subcontinent and Southeast Asia, producing heavy rainfall events in nearby countries (Figure 1(a)), the period known as the Indian Summer Monsoon (ISM) (Webster *et al.*, 1998; Wang, 2005). As the ISM precipitation accounts for almost 90% of the total annual rainfall, it exerts a significant impact on agriculture and livelihoods of over a billion people. One of the most important characteristics of the ISM is its intraseasonal variability of deep convection and precipitation (Lawrence and Webster, 2001; Goswami, 2005; Goswami and Ajayamohan, 2001, Figure 1(b)), for which the wet and dry conditions occur intermittently every 2–3 weeks (Vecchi and Harrison, 2002). The intraseasonal rainfall variability accounts for nearly 80% of the total variability in the Bay of Bengal (BoB) in JJAS (Figure 1(c)). Since the rainfall variability in the BoB is strongly coupled with the upper ocean processes, we expect that the sea surface temperature (SST) and surface heat fluxes significantly influence the characteristics of the intraseasonal rainfall variability (e.g. Lawrence and Webster, 2001). Indeed, a number of observational and modeling studies have examined the intraseasonal relationship between SST and rainfall, showing that the intraseasonal SST warming precedes the deep convection and heavy precipitation (Sengupta *et al.*, 2001; Vecchi and Harrison, 2002; Fu *et al.*, 2003; Seo *et al.*, 2014; Xi *et al.*, 2015).

On the interannual time scale, tropical Indian Ocean SST substantial variability associated with the Indian Ocean Dipole (IOD). The IOD is characterized by an anomalous warming or cooling in the southeastern Indian Ocean, accompanied by an SST anomaly of the opposite sign in the western Indian Ocean, during the negative or positive phase of the IOD, respectively (Saji *et al.*, 1999; Murtugudde and Busalacchi, 1999; Webster *et al.*, 1999, Figure 3). The impact of the IOD on the ISM rainfall has been well established (e.g. Ashok *et al.*, 2001, 2004; Gadgil *et al.*, 2004; Ihara *et al.*, 2007; Ummenhofer *et al.*, 2011). As the IOD switches its phase, the change in the background SST modulates the strength of the ocean-atmosphere coupling, intraseasonal convection, and thus the monsoon circulation over the BoB (Ajayamohan *et al.*, 2008). The IOD also modulates the well-known teleconnection between the El Niño-Southern Oscillation (ENSO) and the ISM (Ashok *et al.*, 2004; Ihara *et al.*, 2007; Ummenhofer *et al.*, 2011).

A key question of the study is how the intraseasonal rainfall variability and its coupling with the BoB ocean are modulated by the IOD. In this study, the impact of ENSO is not rigorously considered, as previous studies demonstrated that ENSO tends to be relatively uncorrelated with summertime intraseasonal convective variability in the BoB (Lawrence and Webster, 2001; Ajayamohan *et al.*, 2008). Nevertheless, additional

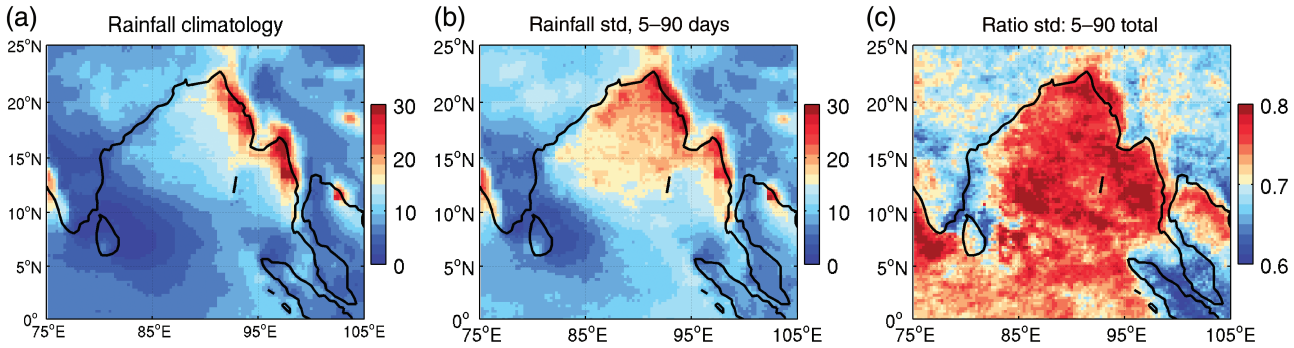

Figure 1. (a) JJAS rainfall climatology (mm day^{-1}) from TRMM 3B42 (1998–2015). (b) SD of the 5–90 day filtered JJAS rainfall, and (c) the ratio between the SD of 5–90 day filtered JJAS rainfall to SD of the unfiltered rainfall.

analysis has been carried out that isolates the IOD influences from that of ENSO, and the results are provided in the Supporting information.

The article is organized as follows: Section 2 describes the data and methodology. Section 3 presents the results investigating the intraseasonal air–sea interaction in Section 3.1 and its interannual variability in Section 3.2, followed by the atmospheric moisture budget analysis in Section 3.3. Section 4 is a summary and discussion of implications.

2. Data and methodology

We use the daily precipitation estimate from the Tropical Rainfall Measuring Mission (TRMM) version 3B42 on a 0.25° × 0.25° grid for 1998–2015 (Huffman *et al.*, 2007). We also use the Global Precipitation Climatology Project (GPCP) 1° daily rainfall product version 1.2 (Huffman *et al.*, 2001) for the period of 1997–2015. For the SST, the 0.25° daily NOAA Optimum Interpolation SST analysis (Reynolds *et al.*, 2007) is used. The latent heat (LH) flux for the same period is taken from the daily objectively-analyzed air-sea fluxes (OAFlux) version 3 (Yu and Weller, 2007). The column-integrated moisture budget analysis is based on the National Centers for Environmental Prediction-National Center for Atmospheric Research reanalysis dataset (Kalnay *et al.*, 1996). The time period of the analysis is restricted to 1998–2015 due to the availability of TRMM rainfall data. To investigate the intraseasonal variations of oceanic and atmospheric properties, the data are filtered using 5–90-day Butterworth band-pass filtering (e.g. Xi *et al.*, 2015).

3. Analysis and results

3.1. Intraseasonal SST-LH-rainfall relationship

To examine the evolution of the ocean-atmosphere fields in association with the intraseasonal rainfall variability, this study adopts the approach by Xi *et al.* (2015) and extends the analysis to 2015. Specifically, lagged composite anomalies for SST, wind speed (WS), and rainfall are constructed for ±25 days around the onset of the heavy intraseasonal rainfall events. Heavy or extreme rainfall events are defined as when the intraseasonal precipitation anomaly averaged over the BoB (15°–23°N, 85°–95°E) exceeds one standard deviation (SD). If two intraseasonal rainfall events take place <10 days apart, they are considered as one event. This way, we obtained a total of 83 heavy intraseasonal rain events for the period of JJAS 1998–2015.

Figure 2(a) shows the zonally averaged (85°–95°E) lagged composite evolutions of the intraseasonal anomalies against the intraseasonal heavy rainfall peaks. The SST warming emerges north of 10°N about 10–15 days before the onset of the precipitation, with the maximum SST found at 15°N about approximately 5-days before the peak. This pre-convection period is quiescent, with anomalously negative WS and LH anomalies leading to the warming of the sea surface. The transition from the positive to negative SST anomaly occurs on Day 0 at 18°N and around Day 2 north of 18°–22°N. This period corresponds to the arrival of the intraseasonal convective anomaly, accompanied by the maximum positive LH and WS anomalies (Figure 2(b)). The enhanced moisture transfer to the atmosphere then facilitates the extreme precipitation events. During and after the peak rainfall, the heat loss from the sea surface through evaporation and upper ocean mixing results in SST cooling that lasts for >+10 days (Sengupta and Ravichandran, 2001; Sengupta *et al.*, 2001). These northward propagating intraseasonal anomalies and their phase relationships are driven by the monsoon intraseasonal variability inherent to the summer atmospheric circulation over the ISM region (e.g. Goswami, 1998; Jiang *et al.*, 2004). However, recent studies (e.g. Fu *et al.*, 2003, 2007) also suggest the leading role of the SST anomalies and air–sea interaction in the northward propagation of the intraseasonal disturbances in rainfall and clouds over the ISM region (Yasunari, 1979, 1980; Sikka and Gadgil, 1980). This is discussed in the following section.

3.2. Modulation of the intraseasonal ocean-atmosphere coupling by the IOD

How does this intraseasonal air-sea coupling vary interannually in association with the IOD? To answer this,

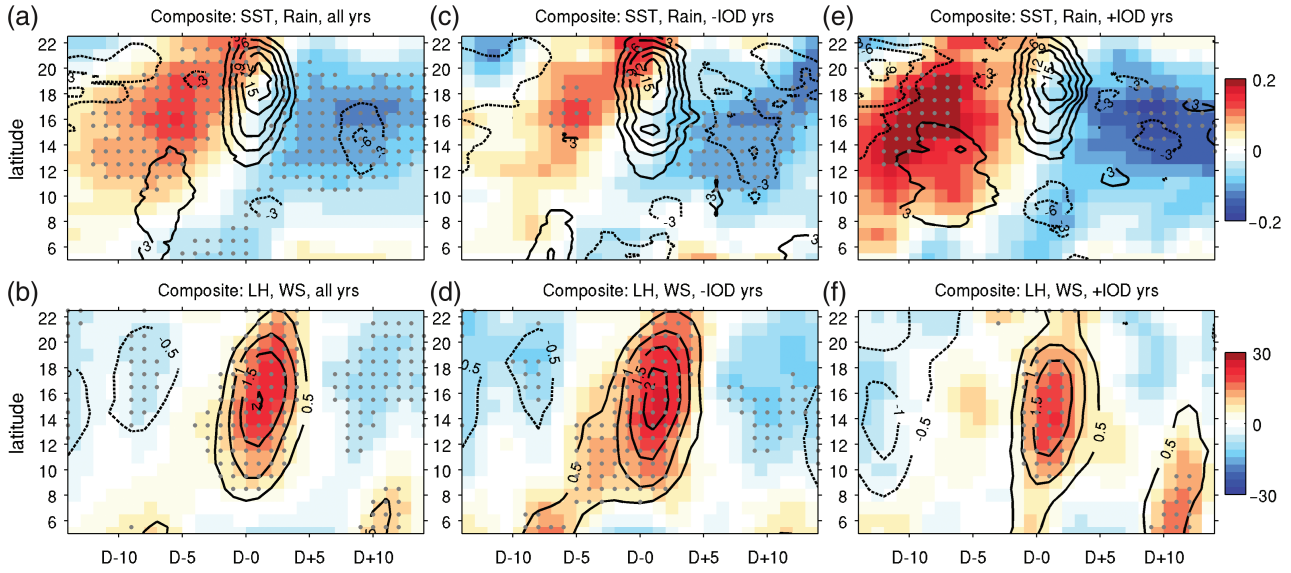

Figure 2. Lagged composite evolutions of the 5–90 day filtered (a) SST (color, °C) and rainfall (contours, mm day^{-1}) and (b) LH (shading, Wm^{-2}, positive out of the ocean) and WS (ms^{-1}, contours) associated with the extreme intraseasonal rainfall events. The extreme intraseasonal rainfall events are defined as when the normalized 5–90 day rainfall averaged over 15°–23°N, 85°–95°E exceeds +1 SD. From this definition, a total of 83 extreme intraseasonal rainfall events are identified for the whole period of 1998–2015. During the +IOD (−IOD) years, there are 22 (26) heavy rain events. Gray dots denote 90% significance level based on a two-sided *t*-test.

conditional lagged composite anomalies are calculated following the phase of the IOD. The years in which negative or positive phases of IOD take place were identified using the JJAS Dipole Mode Index (DMI) following Saji *et al.* (1999). The JJAS DMI index is defined as the difference of the area-averaged JJAS SST anomalies between the western (10°S–10°N, 50°–70°E) and the southeastern (10°S–EQ, 90°–110°E) equatorial Indian Ocean (Figure 3). Negative and positive IOD years are defined as those when JJAS DMI > 0.75 SD and DMI < −0.75 SD, respectively (e.g. Cai *et al.*, 2013). With such criteria, a total of six negative IOD years (1998, 2001, 2005, 2010, 2013, and 2014) and five positive IOD years (2003, 2007, 2008, 2012, and 2015) are obtained (Table 1). Among these years, the year 2015 is classified as El Niño, while 1998 and 2010 are La Niña according to the Climate Prediction Center Oceanic Niño Index. Thus, the composite analysis is repeated for the 'pure' IOD years where IOD years that coincided with ENSO years are excluded in the analysis. The result for the latter is, in general, similar to the former (the supplementary figures), which is consistent with the finding from Ajayamohan *et al.* (2008, 2009). Therefore, to keep the sample size not too small for the significance testing, the analysis in this study is based on the IOD index. The statistical significance of the composite anomalies is assessed by a Student's *t*-test. Unless otherwise noted, the gray dots in the figures will denote the areas of 90% confidence level.

The spatial distributions of the composite SST anomalies during −IOD and +IOD years are shown in Figure 3. In addition to the reversal of the east-west SST contrast on the equator in the opposite phases of the IOD, the composite SST fields show that the BoB experiences moderately warm (cold) SST anomaly in −IOD (+IOD) years. As the local SST condition is strongly coupled to the intraseasonal rainfall variability in the BoB through LH, one would expect a distinctive SST–rainfall relationship over BoB in different IOD years. This is hinted at in Figure 4, which compares the SD of the JJAS intraseasonal rainfall for −IOD and +IOD years. It shows that the intraseasonal rainfall variability is more pronounced during the −IOD years, especially over the northern BoB. An examination of the difference in rainfall variability for the pure IOD years yields very similar results (Figure S1). The enhancement of the intraseasonal rainfall variability motivates us to re-examine the composite evolution of the SST, LH, and WS in relation to intraseasonal rainfall separately for −IOD and +IOD years.

The results are shown in Figures 2(c)–(f). Across the BoB (north of 10°N), the pre-convection SST warming and the post-convection SST cooling tend to be noticeably weaker in −IOD years compared to +IOD years. Both the composites show the northward propagating SST anomalies, but the SST warming peaks at about 5–6 days before the peak in −IOD years, as opposed to 10–15 days prior in +IOD years. Ajayamohan *et al.* (2008) showed that, during the −IOD years, the pre-convection SST warming is weaker, and the intraseasonal SST variability has a shorter period north of 10°N (their Figure 13). The corresponding LH and WS anomalies are, however, much more pronounced prior to and during the peak rainfall events in −IOD years, with the clearer northward propagating characteristics from the equatorial southeastern Indian Ocean toward the BoB (Ajayamohan *et al.*, 2008).

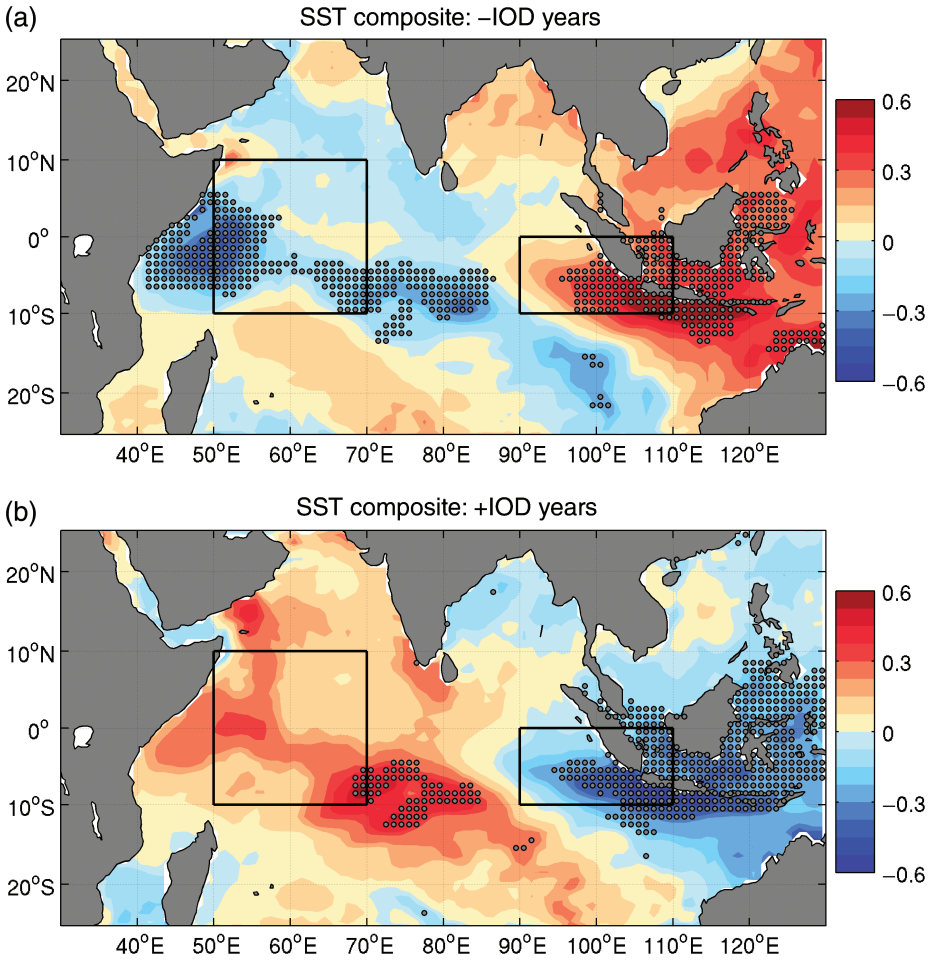

Figure 3. JJAS SST anomaly patterns associated with the (a) −IOD and (b) +IOD years. The boxes indicate the western (10°S–10°N, 50°–70°E) and southeastern (10°S–10°N, 50°–70°E) equatorial Indian Ocean used to construct the JJAS DMI (Saji *et al.*, 1999). Gray dots denote 95% significance level in SST anomaly based on a two-sided *t*-test.

Recalling that the Bay-wide local SST anomaly during the −IOD years is weakly positive (Figure 3), the amplified LH and WS anomalies indicate that the reduced SST intraseasonal variability is a result of stronger heat flux damping, which is in turn conducive to stronger intraseasonal rainfall events. In contrast, in +IOD years, the LH and WS anomalies associated with the rainfall events are weaker, and the northward propagating characteristics are less coherent. This difference in the level of intraseasonal rainfall variability is consistent with Figure 3. The same analysis is repeated for the pure IOD years, showing that the results remain largely similar (Figure S2).

3.3. Moisture budget analysis

The difference of the characteristics of the intraseasonal rainfall events during the −IOD and +IOD years is further examined via column-integrated moisture budget analysis (Hsu and Li, 2012; Hsu *et al.*, 2013; Xi *et al.*, 2015),

$$\frac{\partial q}{\partial t} = -\left(\vec{V}_H \cdot \vec{\nabla}_H q\right) - \left(q\nabla \cdot \vec{V}_H\right) - \frac{\partial}{\partial p}(\omega q) - \frac{Q_2}{L} \quad (1)$$

Table 1. The chosen +IOD and −IOD years for the period of 1988–2015. +IOD (−IOD) years are defined in this study as the years when the JJAS DMI is greater than (less) than +0.75 SD (−0.75 SD). The JJAS DMI is defined as the difference of the JJAS SST anomaly between the western tropical Indian Ocean (50°–70°E, 10°S–10°N) and tropical southeastern Indian Ocean (90°–110°E, 10°S–0°N). The years with an asterisk denote the IOD years that coincide with ENSO based on JJAS ENSO index (http://www.cpc.ncep.noaa.gov/products/analysis_monitoring/ensostuff/ensoyears.shtml).

IOD+	IOD−
2003	1998*
2007	2001
2008	2005
2012	2010*
2015*	2013
	2014

where q is specific humidity, $\vec{V}_H$ the horizontal velocity vectors, $\vec{\nabla}_H$ the horizontal gradient operator, ω the pressure vertical velocity, Q_2 the atmospheric apparent moisture sink (Yanai *et al.*, 1973; Johnson *et al.*, 2015), and L the latent heat of condensation. The rate of change of the moisture on the left-hand side of Equation (1)

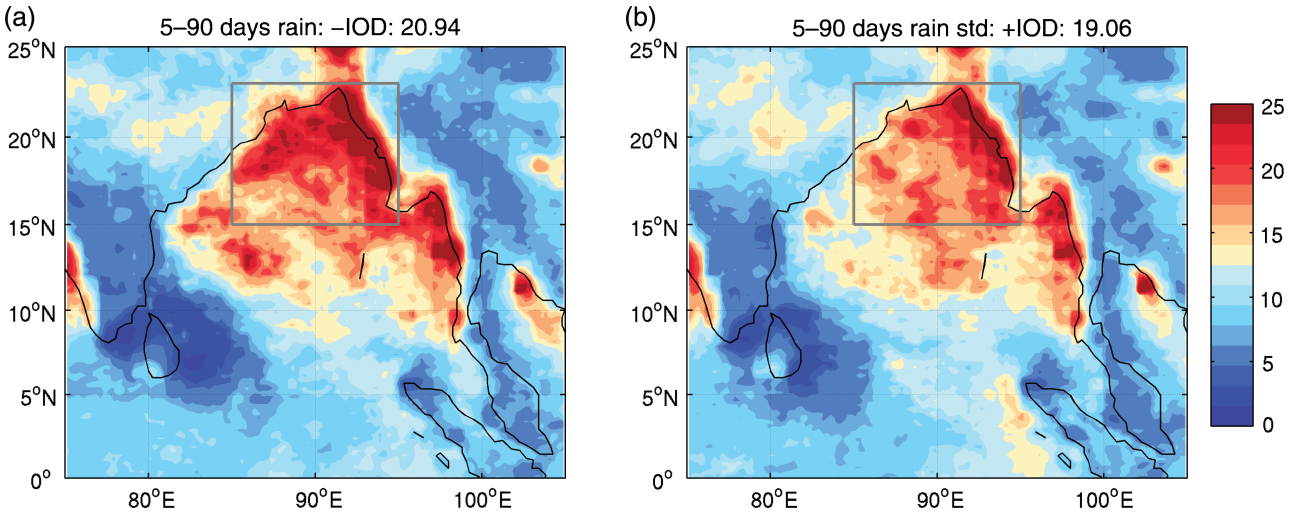

Figure 4. Map of mean SD of the 5–90 day filtered rainfall (mm day^{-1}) for the –IOD and +IOD years. Mean SD value averaged over the gray box is denoted in the title.

is balanced by the terms on the right. The first term is the horizontal moisture advection, and the second and the third are the horizontal moisture convergence and vertical moisture flux, respectively, which together represent the vertical moisture advection. The last term represents the loss of moisture out of the air column as condensation into the rain. In this analysis, this term is obtained as the residual, and thus it also includes other processes that are not fully resolved from the daily data as well as numerical errors due to finite differencing. Each term in Equation (1) is integrated from 1000 to 300 hPa.

The composite evolutions of each term averaged during the peak rainfall period are shown in the top panel of Figure 5, as well as those for the –IOD and +IOD years in the middle and lower panels. The total moisture rate is close to zero (not shown), indicating the quasi-equilibrium state during the peak of the heavy rainfall event. The greatest source of moisture in the atmospheric column over the BoB is the horizontal convergence of moisture, which is largest at the lower level near the sea surface (Figure S3). The vertical flux also adds additional moisture to the air column but is of secondary importance. In the northern BoB, the moisture increase through the horizontal convergence is mostly balanced by the moisture loss through condensation and rainfall. This moisture addition and removal processes are most pronounced in the northern BoB. The horizontal advection also accounts for the loss of moisture but occurs over the broad area over the BoB.

Evidently, the horizontal advection terms do not vary appreciably during the different phases of the IOD (Figures 5(e) and (i)), especially in the northern BoB, where the intraseasonal rainfall variability is most pronounced. In this region, the principal balance during the –IOD years is between the increased horizontal moisture convergence and the increased condensational loss (Figure 5). The increase in moisture convergence is most pronounced in the lower atmosphere below 700 hPa with the peak at 925 hPa (Figure S3), suggesting the critical role of greater moistening of the lower troposphere by the evaporation during the –IOD years. In contrast, the moisture convergence in +IOD years is weakened mostly in the lower level. The enhanced vertical moisture flux does not exhibit large changes. Hence, the stronger low-level moisture convergence associated with the warmer SST and increased LH flux in –IOD years (Figure 2(d)) leads to the stronger intraseasonal precipitation events in the northern BoB (Kemball-Cook and Wang, 2001; Jiang *et al.*, 2004).

The role of SST rise in the intraseasonal moisture convergence is further illustrated in Figure 6 showing the lag correlation between the SST and moisture convergence over the northern BOB. For all years (black), the SST and moisture convergence are correlated most significantly when the former leads (lags) the latter by about 7 days (10 days). This quadrature phase relationship implies coherent intraseasonal variability with a period of approximately 40 days. Furthermore, the lag correlation is enhanced during the –IOD years (orange) compared to +IOD years (blue). This lends further support to the notion that the SST warming during the pre-convection period is important for the intensity of intraseasonal rainfall during the –IOD years.

4. Conclusions and discussions

This study examines the coupling of the intraseasonal rainfall events with the SST in the BoB and its interannual modulation of the intraseasonal rainfall variability. Based on the lagged composite analysis, it is shown that the ocean–atmosphere coupling on the intraseasonal time scale is significant, especially in the northern BoB, with LH playing a key role as the communicator. On average, the maximum warming in SST precedes the peak in precipitation by approximately

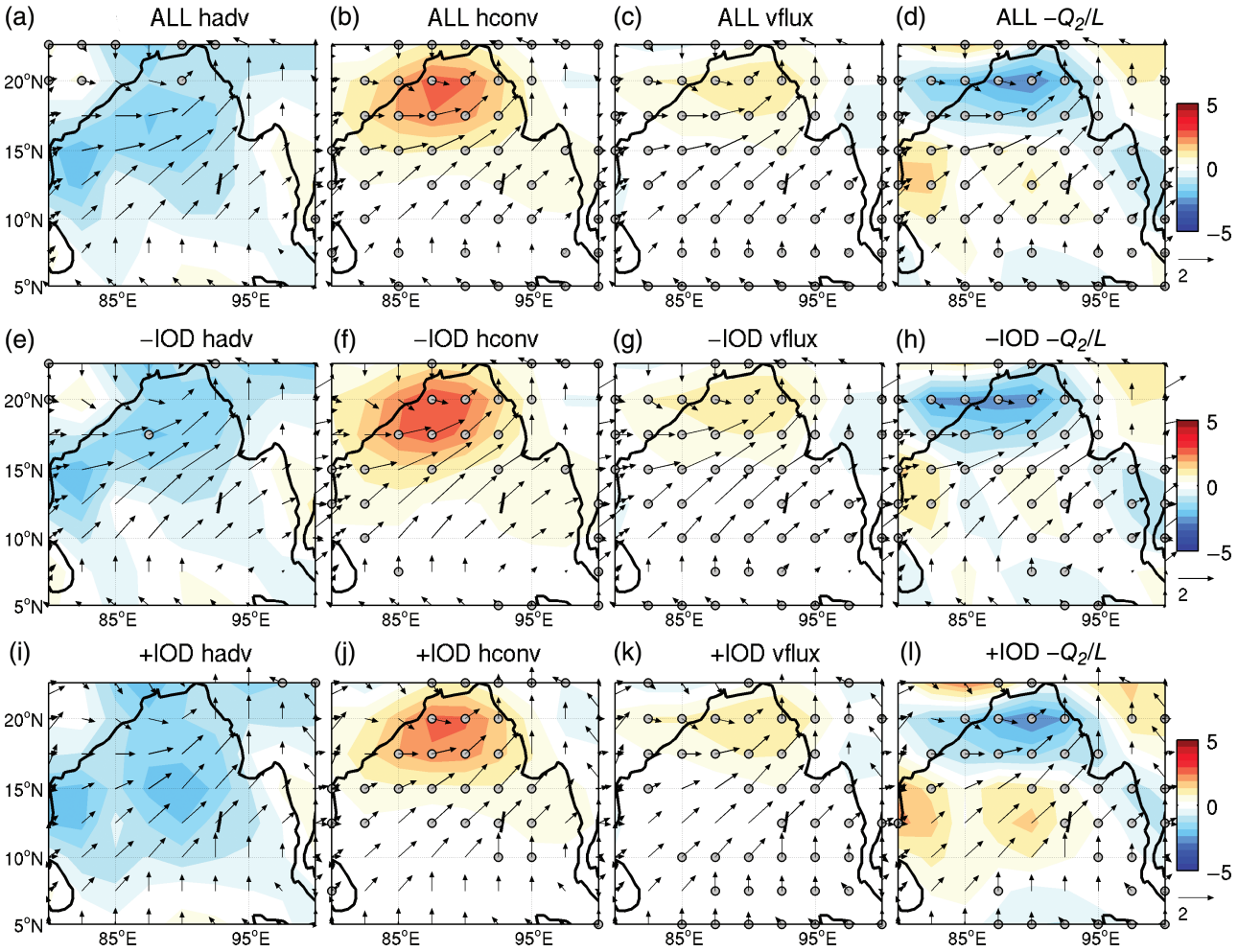

Figure 5. The column-integrated (1000–300 hPa) moisture budget terms (kg m^{-2} day^{-1}) averaged during Day 0–2, showing (from left to right) horizontal moisture advection, horizontal moisture convergence, vertical moisture flux, and the moisture loss due to condensation. Vectors are composite anomalies of the 5–90 day filtered 1000 hPa winds. Gray dots denote the 90% significance level of the composite anomalies.

5 days in the northern BoB. In addition, the coherent northward propagating anomalies of SST and LH are observed, suggesting that they are coupled to the northward propagating convection and clouds over the ISM region.

The intraseasonal ocean-atmosphere coupling is strongly modulated by the IOD. With the use of the JJAS DMI, a total of six years, out of the 1998–2015 TRMM data period, are identified as −IOD years, and five as +IOD years. Despite the relatively small number of the chosen IOD years due to the short satellite data record, the clear distinction in the ocean-atmosphere coupling patterns in different phases of the IOD can be observed. In −IOD years when the BoB SST is anomalously warm, the intraseasonal variability of LH and WS are enhanced, facilitating the stronger moisture transfer to the atmosphere, leading to strengthened intraseasonal rainfall variability. This is supported by the column-integrated moisture budget analysis showing that, indeed in −IOD years, the horizontal moisture convergence, the primary source of moisture during the intraseasonal rainfall peak, is significantly strengthened in the lower atmosphere (below 750 hPa) over the northern BoB. The resultant stronger vertical moisture advection predominantly balances the increased rainfall variability in −IOD years in the northern BoB.

The same analysis is repeated using the GPCP 1° daily rainfall dataset to confirm the robustness of the finding based on the TRMM 3B42. Overall, the key conclusion of the study is not sensitive to the choice of the dataset. For example, the elevated level of intraseasonal rainfall variability in the BoB in the −IOD years compared to the +IOD years. Therefore, the intraseasonal SST-rainfall coupling in the northern BoB and its modulation by the IOD is significant and robust. The fact that SST leads rainfall during the summer monsoons provides important predictive information on the onset of the monsoon rainfall and its active/break cycles over the BoB and surrounding land areas. This relationship varies with the large-scale mode of variability in the IOD, with implications for predictions on the interannual time scale. In particular, −IOD years exhibit enhanced intraseasonal rainfall variability over Bangladesh and into Myanmar, while +IOD years show increased variability over northern India.

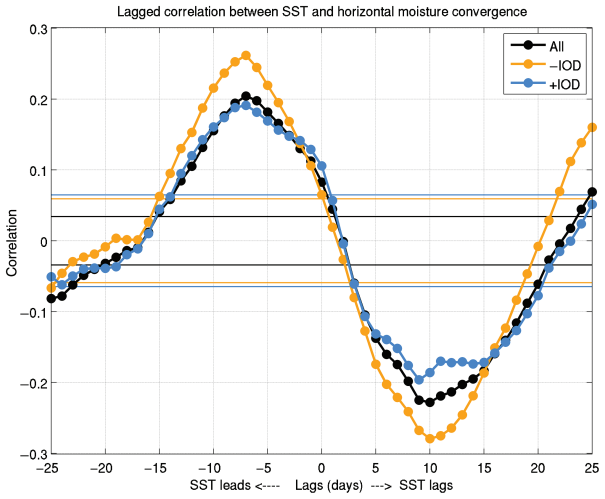

Figure 6. Lagged correlations between SST and horizontal moisture convergence averaged over the northern BoB (85°–95°E, 15°–25°N), color-coded to represent the correlations during all, −IOD and +IOD years. The horizontal lines represent the lower and upper 95% confidence bounds for each case.

Acknowledgements

This project is part of SJ's Summer Student Fellowship (SSF) program at Woods Hole Oceanographic Institution (WHOI) sponsored by the National Science Foundation Research Experience for Undergraduates Program (NSF-REU). HS acknowledges grants from the Office of Naval Research (N00014-15-1-2588) and National Oceanic and Atmospheric Administration (NA15OAR4310176). CCU acknowledges support from the National Science Foundation under AGS-1304245. The authors thank two anonymous reviewers for their constructive comments, which helped to substantially improve the manuscript.

Supporting information

The following supporting information is available:

Figure S1. As in Figure 3, but for pure IOD years. Mean SD value averaged over the gray box is denoted in the title.

Figure S2. As in Figure 2, but for pure IOD years. During the pure +IOD (pure −IOD) years, there are 18 (16) heavy rain events.

Figure S3. Vertical profiles of the horizontal moisture convergence (10^{-3} kg m^{-2} day^{-1}) averaged during the peak rainfall event for all (black), +IOD (blue) and −IOD (orange) years.

Figure S4. As in Figure 3 but using the GPCP 1° daily rainfall estimate from 1997 to 2015. Mean SD value averaged over the gray box is denoted in the title.

References

Ajayamohan RS, Rao SA, Yamagata T. 2008. Influence of Indian Ocean Dipole on poleward propagation of boreal summer intraseasonal oscillations. *Journal of Climate* **21**: 5437–5454.

Ajayamohan RS, Rao SA, Luo J-J, Yamagata T. 2009. Influence of Indian Ocean Dipole on boreal summer intraseasonal oscillations in a coupled general circulation model. *Journal of Geophysical Research* **114**: D06119.

Ashok K, Guan Z, Yamagata T. 2001. Impact of the Indian Ocean Dipole on the relationship between the Indian monsoon rainfall and ENSO. *Geophysical Research Letters* **28**: 4499–4502.

Ashok K, Guan Z, Saji NH, Yamagata T. 2004. Individual and combined influences of the ENSO and Indian Ocean Dipole on the Indian summer monsoon. *Journal of Climate* **17**: 3141–3155.

Cai W, Zheng X-T, Weller E, Collins M, Cowan T, Lengaigne M, Yu W, Yamagata T. 2013. Projected response of the Indian Ocean Dipole to greenhouse warming. *Nature Geoscience* **6**: 999–1007.

Fu X, Wang B, Li T, McCreary JP. 2003. Coupling between northward-propagating, intraseasonal oscillations and sea surface temperature in the Indian Ocean. *Journal of Atmospheric Science* **60**: 1733–1753.

Fu X, Wang B, Waliser DE, Tao L. 2007. Impact of atmosphere–ocean coupling on the predictability of monsoon intraseasonal oscillations. *Journal of Atmospheric Science* **64**: 157–174.

Gadgil S, Vinayachandran PN, Francis PA, Gadgil S. 2004. Extremes of the Indian summer monsoon rainfall, ENSO and equatorial Indian Ocean oscillation. *Geophysical Research Letters* **31**: L12213.

Goswami BN. 1998. Interannual variations of Indian summer monsoon in a GCM: external conditions versus internal feedbacks. *Journal of Climate* **11**: 501–522.

Goswami BN. 2005. South Asian monsoon. In *Intraseasonal Variability in the Atmosphere-Ocean Climate System*, Lau WKM, Waliser DE (eds). Praxis Springer: Chichester, UK; 19–61.

Goswami BN, Ajayamohan RS. 2001. Intraseasonal oscillations and interannual variability of the Indian summer monsoon. *Journal of Climate* **14**: 1180–1198.

Hsu P-C, Li T. 2012. Role of the boundary layer moisture asymmetry in causing the eastward propagation of the Madden-Julian Oscillation. *Journal of Climate* **25**: 4914–4931.

Hsu P-C, Li T, Murakami H, Kitoh A. 2013. Future change of the global monsoon revealed from 19 CMIP5 models. *Journal of Geophysical Research – Atmospheres* **118**: 1247–1260.

Huffman GJ, Adler RF, Morrissey MM, Curtis S, Joyce R, McGavock B, Susskind J. 2001. Global precipitation at one-degree daily resolution from multi-satellite observations. *Journal of Hydrometeorology* **2**: 36–50.

Huffman GJ, Adler RF, Bolvin DT, Gu G, Nelkin EJ, Bowman KP, Hong Y, Stocker EF, Wolff DB. 2007. The TRMM multi-satellite precipitation analysis: quasi-global, multi-year, combined-sensor precipitation estimates at fine scale. *Journal of Hydrometeorology* **8**: 38–55.

Ihara C, Kushnir Y, Cane MA, De la Pena VH. 2007. Indian summer monsoon rainfall and its link with ENSO and Indian Ocean climate indices. *International Journal of Climatology* **27**: 179–187.

Jiang X, Li T, Wang B. 2004. Structures and mechanisms of the northward propagating boreal summer intraseasonal oscillation. *Journal of Climate* **17**: 1022–1039.

Johnson RH, Ciesielski PE, Ruppert JH Jr. 2015. Sounding-based thermodynamic budgets for DYNAMO. *Journal of Atmospheric Science* **72**: 598–622.

Kalnay E, Kanamitsu M, Kistler R, Colling W, Deaven D, Gandin L, Iredell M, Saha S, White G, Wollen J, Zhu Y, Chelliah M, Ebisuzaki W, Higgins W, Janowiak J, Mo KC, Ropelewski C, Wang J, Leetmaa A, Reynolds R, Jenne R, Joseph D. 1996. The NCEP/NCAR 40-year reanalysis project. *Bulletin of the American Meteorological Society* **77**: 437–470.

Kemball-Cook SR, Wang B. 2001. Equatorial waves and air– sea interaction in the boreal summer intraseasonal oscillation. *Journal of Climate* **14**: 2923–2942.

Lawrence DM, Webster PJ. 2001. Interannual variations of the intraseasonal oscillation in the South Asian summer monsoon region. *Journal of Climate* **14**: 2910–2922.

Murtugudde R, Busalacchi AJ. 1999. Interannual variability of the dynamics and thermodynamics of the tropical Indian Ocean. *Journal of Climate* **12**: 2300–2326.

Reynolds RW, Smith TM, Liu C, Chelton DB, Casey KS, Schlax MG. 2007. Daily high-resolution-blended analyses for sea surface temperature. *Journal of Climate* **20**: 5473–5496.

Saji NH, Goswami BN, Vinayachandran PN, Yamagata T. 1999. A dipole mode in the tropical Indian Ocean. *Nature* **401**: 360–363.

Sengupta D, Ravichandran M. 2001. Oscillations of Bay of Bengal sea surface temperature during the 1998 summer monsoon. *Geophysical Research Letters* **28**: 2033–2036.

Sengupta D, Senan R, Goswami BN. 2001. Origin of intraseasonal variability of circulation in the tropical central Indian Ocean. *Geophysical Research Letters* **28**: 1267–1270.

Seo H, Subramanian AC, Miller AJ, Cavanaugh NR. 2014. Coupled impacts of the diurnal cycle of sea surface temperature on the Madden-Julian Oscillation. *Journal of Climate* **27**: 8422–8443.

Sikka DR, Gadgil S. 1980. On the maximum cloud zone and the ITCZ over Indian longitude during southwest monsoon. *Monthly Weather Review* **108**: 1840–1853.

Ummenhofer CC, Sen Gupta A, Li Y, Taschetto AS, England MH. 2011. Multi-decadal modulation of the El Niño-Indian monsoon relationship by Indian Ocean variability. *Environmental Research Letters* **6**: 034006.

Vecchi GA, Harrison DE. 2002. Monsoon breaks and subseasonal sea surface temperature variability in the Bay of Bengal. *Journal of Climate* **15**: 1485–1493.

Wang B. 2005. Theory. In *Intraseasonal Variability in the Atmosphere-Ocean Climate System*, Lau WKM, Waliser DE (eds). Praxis Springer: Chichester, UK; 307–360.

Webster PJ, Magana VO, Palmer TN, Shukla J, Romas RA, Yanai M, Yasuniari T. 1998. Monsoons: processes, predictability, and the prospects for prediction. *Journal of Geophysical Research* **13**: 14451–14510.

Webster PJ, Moore AM, Loschnigg JP, Leben RR. 1999. Coupled ocean-atmosphere dynamics in the Indian Ocean during 1997-98. *Nature* **401**: 356–360.

Xi J, Zhou L, Murtugudde R, Jiang L. 2015. Impacts of intraseasonal SST anomalies on precipitation during Indian summer monsoon. *Journal of Climate* **28**: 4561–4575.

Yanai M, Esbensen S, Chu J-H. 1973. Determination of bulk properties of tropical cloud clusters from large-scale heat and moisture budgets. *Journal of Atmospheric Science* **30**: 611–627.

Yasunari T. 1979. Cloudiness fluctuation associated with the Northern Hemisphere summer monsoon. *Journal of the Meteorological Society of Japan* **57**: 227–242.

Yasunari T. 1980. A quasi-stationary appearance of 30–40 day period in the cloudiness fluctuation during summer monsoon over India. *Journal of the Meteorological Society of Japan* **58**: 225–229.

Yu L, Weller RA. 2007. Objectively analyzed air-sea heat fluxes (OAFlux) for the global ice-free oceans. *Bulletin of the American Meteorological Society* **88**: 527–539.

Supplementary Information for

Intraseasonal rainfall variability in the Bay of Bengal during the Summer Monsoon: Coupling with the ocean and modulation by the Indian Ocean Dipole

Siraput Jongaramrungruang[1,2], Hyodae Seo[2], and Caroline C. Ummenhofer[2]

Trinity College, University of Cambridge, Cambridge, United Kingdom

Physical Oceanography Department, Woods Hole Oceanographic Institution

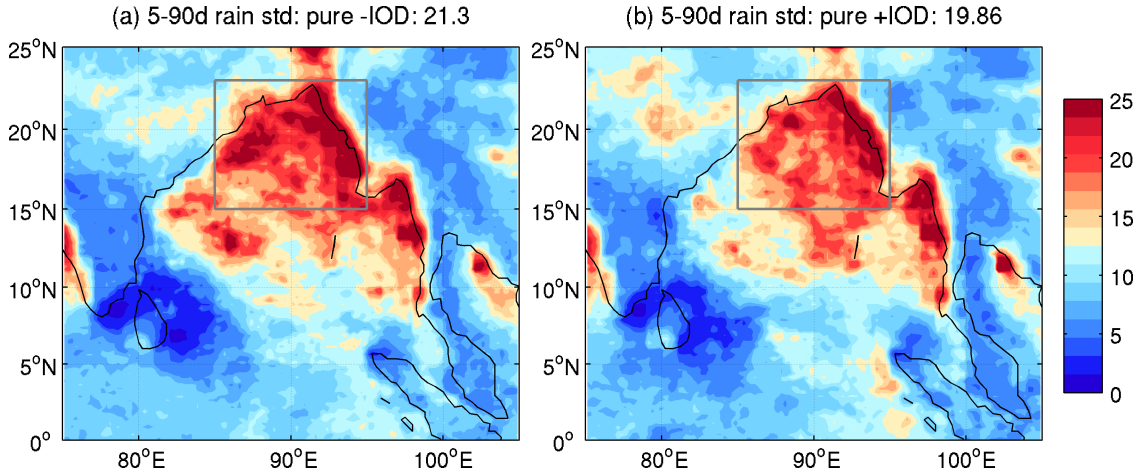

Figure S1 As in **Figure 3**, but for pure IOD years. Mean SD value averaged over the gray box is denoted in the title.

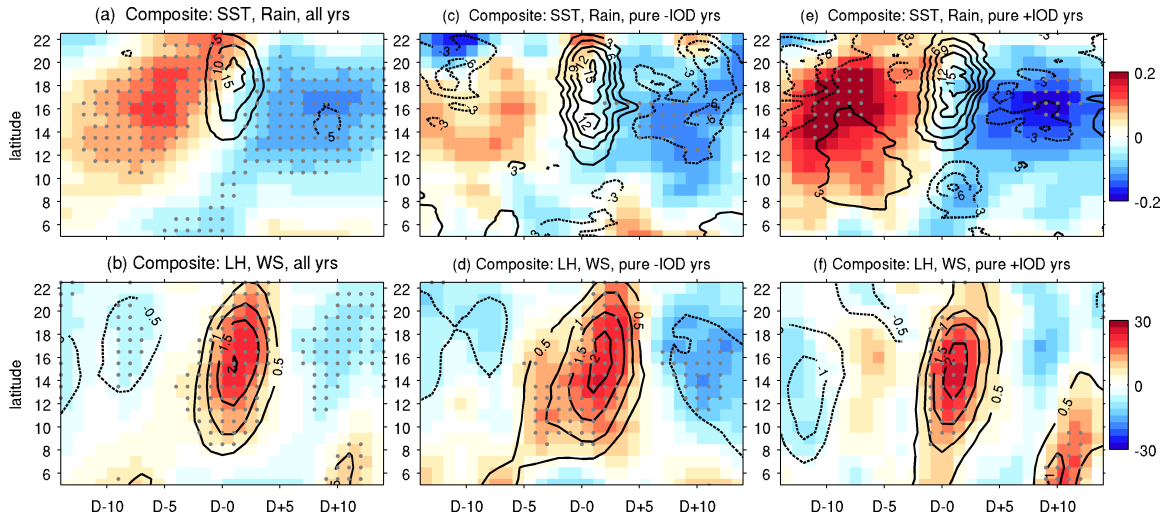

Figure S2 As in **Figure 2**, but for pure IOD years. During the pure +IOD (pure -IOD) years, there are 18 (16) heavy rain events.

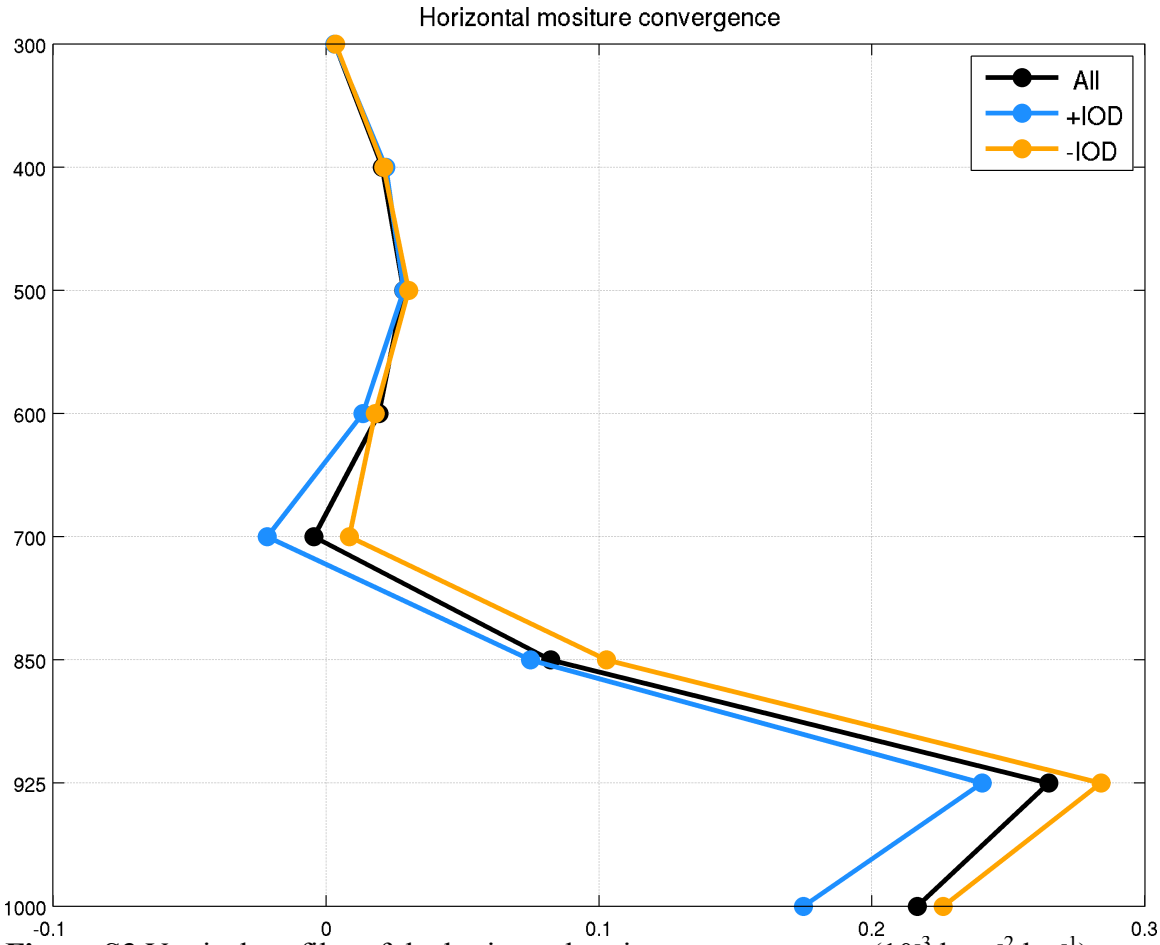

Figure S3 Vertical profiles of the horizontal moisture convergence (10^{-3} $kgm^{-2}day^{-1}$) averaged during the peak rainfall event for all (black), +IOD (blue) and –IOD (orange) years.

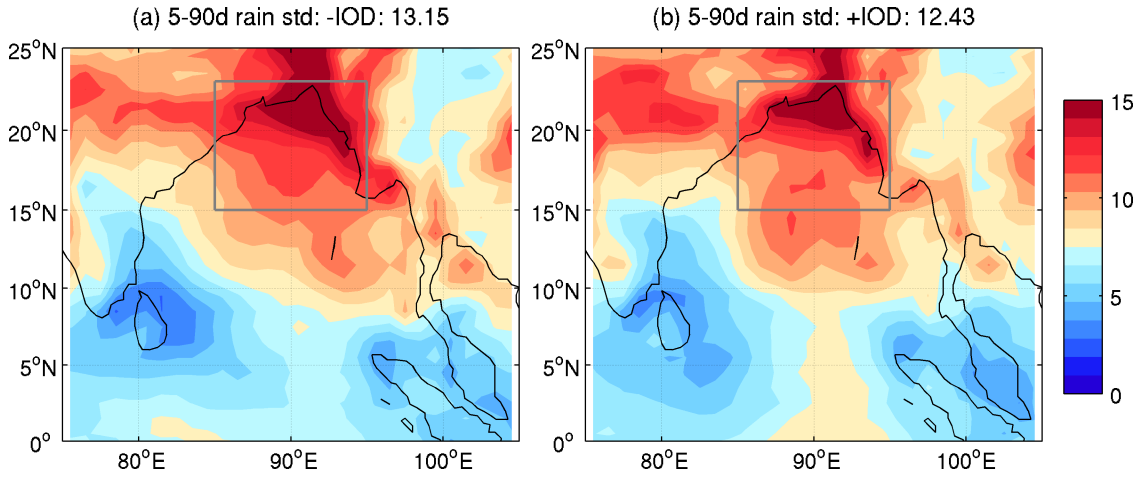

Figure S4 As in **Figure 3** but using the GPCP 1° daily rainfall estimate from 1997-2015. Mean SD value averaged over the gray box is denoted in the title.